

See discussions, stats, and author profiles for this publication at: <https://www.researchgate.net/publication/257793691>

ASTER mapping of limestone formations and study of caves, springs and depressions in parts of Sultanate of Oman

ARTICLE in ENVIRONMENTAL EARTH SCIENCES · APRIL 2014

Impact Factor: 1.77 · DOI: 10.1007/s12665-013-2419-7

CITATIONS

16

READS

177

2 AUTHORS:



Sankaran Rajendran

Sultan Qaboos University

83 PUBLICATIONS 175 CITATIONS

[SEE PROFILE](#)



Sobhi Nasir

Sultan Qaboos University

271 PUBLICATIONS 701 CITATIONS

[SEE PROFILE](#)



ASTER spectral sensitivity of carbonate rocks – Study in Sultanate of Oman

Sankaran Rajendran*, Sobhi Nasir

Department of Earth Sciences, Sultan Qaboos University, Al-Khod, 123 Muscat, Oman

Received 30 April 2013; received in revised form 14 November 2013; accepted 24 November 2013

Abstract

Remote sensing satellite data plays a vital role and capable in detecting minerals and discriminating rock types for explorations of mineral resources and geological studies. Study of spectral absorption characters of remotely sensed data are under consideration by the exploration and mining companies, and demonstrating the spectral absorption characters of carbonates on the cost-effective multispectral image (rather than the hyperspectral, Lidar image) for easy understanding of all geologists and exploration communities of carbonates is very much important. The present work is an integrated study and an outcome of recently published works on the economic important carbonate rocks, includes limestone, marl, listwaenites and carbonatites occurred in parts of the Sultanate of Oman. It demonstrates the spectral sensitivity of such rocks for simple interpretation over satellite data and describes and distinguishes them based on the absorptions of carbonate minerals in the spectral bands of advanced spaceborne thermal emission and reflection radiometer (ASTER) for mapping and exploration studies. The study results that the ASTER spectral band 8 discriminates the carbonate rocks due to the presence of predominantly occurred carbonate minerals; the ASTER band 5 distinguishes the limestones and marls (more hydroxyl clay minerals) from listwaenite (hydrothermally altered rock) due to the presence of altered minerals and the ASTER band 4 detects carbonatites (ultramafic intrusive alkaline rocks) which contain relatively more silicates. The study on the intensity of the total absorptions against the reflections of these rocks shows that the limestones and marls have low intensity in absorptions (and high reflection values) due to the presence of carbonate minerals (calcite and dolomite) occurred in different proportions. The listwaenites and carbonatites have high intensity of absorptions (low reflection values) due to the occurrence of Mn-oxide in listwaenites and carbonates apart the influence of major carbonate minerals that occurred predominantly in these rocks. The study of ASTER thermal infrared (TIR) spectral bands distinguished the marls have low emissivity of energy due to the presence of hydroxyl bearing alumina-silicate minerals from the other rocks such as limestones, listwaenites and carbonatites which have high emissivity due to the absence of hydroxyl bearing alumina-silicate minerals and the presence of carbonate minerals and carbonates.

Further, the study demonstrates and confirms the spectral sensitivity of marls and carbonatites. Marls have high reflectivity in ASTER visible near infrared (VNIR) and shortwave infrared (SWIR) spectral bands and low emissivity of energy in ASTER TIR spectral bands due to the presence of hydroxyl bearing alumina-silicate minerals. Carbonatites have low reflectivity in ASTER VNIR-SWIR spectral bands and high emissivity in ASTER TIR spectral bands due to the absence of hydroxyl bearing alumina-silicate minerals and the presence of the carbonate minerals and carbonates. These have been discussed by providing the grey scale color image of 14 ASTER spectral bands of the study sites. The study is based on the interpretation of image spectra of multispectral image conducted to map such economic valuable carbonate rocks. It provides a simple methods and basic knowledge, which are of great help to the geology and exploration communities. It is recommended to the geologists, industrialists, exploration communities of carbonates and mine owners to take up the knowledge for economic exploration of such deposits. Further, the study has proved that the technique is time and cost effective in mapping of such deposits and can be used to the areas which have extremely rugged topography occurred in similar arid region, where difficult to do exhaustive sampling and not reachable for conventional geological mapping.

© 2013 COSPAR. Published by Elsevier Ltd. All rights reserved.

Keywords: Remote Sensing; Carbonate rocks; ASTER; Spectral absorptions; Oman

* Corresponding author. Tel.: +968 24142284.

E-mail addresses: sankaranrajendran@yahoo.com, rajendra@squ.edu.om (S. Rajendran).

1. Introduction

Satellite images are capable in discriminating rock types useful for geological applications and significantly used in identification of mineral resources (Rajendran and Nasir, 2013a; Rajendran et al., 2013, 2011a; Mars and Rowan, 2010; Amer et al., 2010; Gabr et al., 2010; Zhang et al., 2007; Rowan and Mars, 2003; Abrams et al., 1988). Especially, the spectral analyses of remotely sensed data are under consideration of several mining companies for exploration and characterization of economic important carbonate rocks namely limestones, marls, listwaenites and carbonatites. Limestones are mostly formed by calcite and dolomite minerals and widely used in construction material, mortar and cement, fertilizer, and flux for smelting of iron ores (Hamilton et al., 1995). The minerals have significance in petroleum geology in increasing the porosity of reservoir rock by 12% during dolomitization which is more suitable for oil reservoirs (Racey, 2001; Van der Meer, 1994, 1995; Hughes Clarke, 1988). The substitution process of the minerals by other minerals in calc-silicates consisted of garnet and pyroxene produces skarns and granitic rocks which are a source of valuable mineral deposits such as copper, gold, iron, lead, zinc, or tungsten (Van der Meer, 1994, 1995). Marl is a calcium carbonate or lime-rich mud consist mixture of clay (35–65%) and calcium carbonate (65–35%) formed under freshwater conditions (Pettijohn, 1957). It is used mostly for agricultural purposes as soil conditioner or acid soil neutralizing agent. The beds of marlstone are massive and appear to lack an orientated fabric and used as ashlar and rubble stone walling for local buildings, church walls, quoins and buttresses. The occurrence of limestones and marls in parts of Sultanate of Oman are described in different studies (Rajendran and Nasir, 2013b; Rajendran et al., 2011b; Beavington Penny et al., 2006; Jones and Desrochers, 1992) and in “The Geology and Tectonics of the Oman Region”, published by The Geological Society, London, Special publication No. 49 (Robertson et al., 1990).

Listwaenite is a hydrothermal fluids altered serpentized ultramafic rock formed at intermediate-to-low temperature within or near major thrust faults and shear zones. It contains quartz, carbonate minerals (calcite, dolomite and ankerite), mica such as fuchsite, together with sulphides (pyrite, galena) and oxides (hematite, magnetite), cobalt minerals and chromite relicts (Rajendran et al., 2013; Nasir et al., 2007; Kunovl et al., 2007; Tsikouras et al., 2006; Kuleshevich, 1984). The rock is extremely important worldwide, because it is potentially associated with economic minerals including gold, nickel, arsenic, cobalt, wolframite and mercury mineralization (Borojević Šoštarić et al., 2011; Tsikouras et al., 2006; Uçurum and Larson, 1999; Uçurum, 1998; Sherlock and Logan, 1995; Leblanc and Fischer, 1990). Similarly, carbonatites (like bastnaesite) also have more than 50% of carbonates/carbonate minerals (calcite, dolomite, ankerite, sodic/potassic carbonates), with sodic pyroxenes, amphiboles, phlogopite,

apatite, olivine and rare/exotic minerals containing F, Nb, P, Ta, Th, REE, U, V or Zr (Rajendran and Nasir, 2013a; Nasir et al., 2011; Mitchell, 2005; Zurevinski and Mitchell, 2004; David and Noreen, 2001; Groves and Vielreicher, 2001; Wall and Mariano, 1996). These are an economic important rock consists REE concentrates occur as small intrusive bodies (3–5 km in diameter) within larger alkaline complexes characteristics of intraplate margins (Nasir et al. 2011, 2009; Tappe et al., 2009; Ahijado et al., 2005; Zaitsev et al., 1998; Le Roex and Lanyon, 1998).

All carbonate rocks discussed above constitute primarily the carbonate minerals (predominantly of calcite and dolomite) and have potential economic importance. The earlier studies of these rock types have provoked constant interest to map their occurrences, spatial distribution, association, origin and conditions of formation. Literatures review that satellite images acquired by remote sensing technique plays in a vital role and have capability in detecting of carbonate minerals, mapping of carbonate rocks and associated mineralization (Rajendran and Nasir, 2013a,b; Rajendran et al., 2013, 2012, 2011b; Rowan and Mars, 2011; Mars and Rowan, 2010; Enton, 2009; Kervyn et al., 2008; Madani et al., 2008; Ninomiya, 2002; Rowan et al., 1986). However, it is very much important to understand the spectral absorption characters of such rocks having similar major mineralogical compositions and interest to distinguish them for better mapping and exploration in remote sensing technique. Therefore, in the present study, an attempt is made to demonstrate the spectral sensitivity of such carbonate rocks namely limestones of Rusayl and Al Jafnayn (Site. 1), marls occurrences near to Sur (Site. 2), listwaenites of Fanjah (Site. 3) and carbonatites of Musawi (Site. 4) regions of parts of Sultanate of Oman (Fig. 1) and describe them based on characters of minerals absorption in the spectral bands of ASTER satellite data to help geologists and exploration communities. This is an integrated study and outcome of work published recently highlights the importance and use of spectral absorptions of minerals to map such economically important rock types.

2. Geological settings

2.1. Limestones of Rusayl and Al Jafnayn region

The regions in and around of Rusayl and Al Jafnayn (Site. 1; Figs. 1 and 2) mainly consists sedimentary formations of Tertiary and Quaternary age which are underlain by the Allochthonous unit namely Samail nappe. Here, two major Tertiary Formations namely Lower nodular limestones (Lm) and Upper nodular limestones (Ulm) are distributed in centre of the region and the Alluvial fans and Terraces of Recent to Sub-Recent Quaternary Formations are occurred in between them (Fig. 2). The Lower nodular limestone is associated with Fossilized yellow marl formations (Ym-interlayered by brown sandstone and Yml), whereas the Upper nodular limestone is mainly associated with the Recent to Sub-recent Alluvial fan sediments

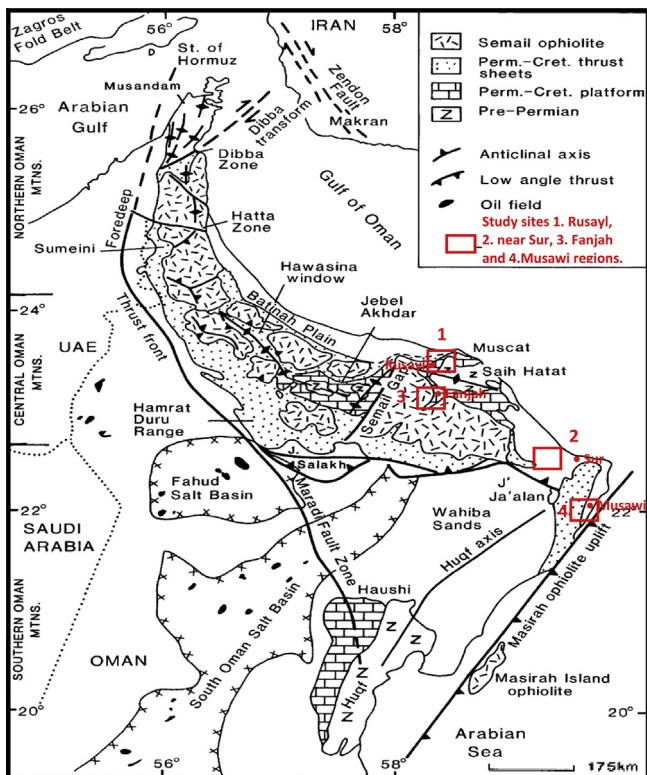


Fig. 1. Regional geology and structure map of the Oman Mountain area (after Robertson and Searle, 1990) shows the study sites (1) Rusayl and Al Jafnayn area, (2) area near to Sur, (3) Fanjah and (4) area around Musawi.

(Rlm). The occurrence and spatial distribution of other sedimentary formations of the area are shown in the Fig. 2. The Sheeted Dyke (SD) namely doleritic and basaltic dykes are occurred in the SW of the region. The prominent occurrences of such limestone formations of this region are chosen in this study as best to discriminate different types of limestones over the satellite data based on spectral sensitivity of limestone bearing minerals.

2.2. Marls near Sur region

The geology around Sur (Site. 2; Figs. 1 and 3) composed of sedimentary rocks of Abat Formations (AF), Jafnayn Formations (JF), Rus Formations (RF) and Seeb Formations (SEF) of Late Paleocene-Early Eocene age (Tertiary Group). The formations are deposited by limestones and marls. Marl is predominant in all the formations (Fig. 3) which are underlain by the Allochthonous units such as Hawasina and Samail nappes and overlain by colluvial sediments of Quaternary age. The occurrences and spatial distributions of other rock types are shown in the Fig. 3 (Rajendran and Nasir, 2013b).

2.3. Listwaenites of Fanjah region

The Fanjah region is situated in the Central Oman Mountains (Site. 3; Figs. 1 and 4) between Jebel Akhdar and Saih Hatah windows expose Parautochthonous rocks through the overlying Allochthons. The region shows a

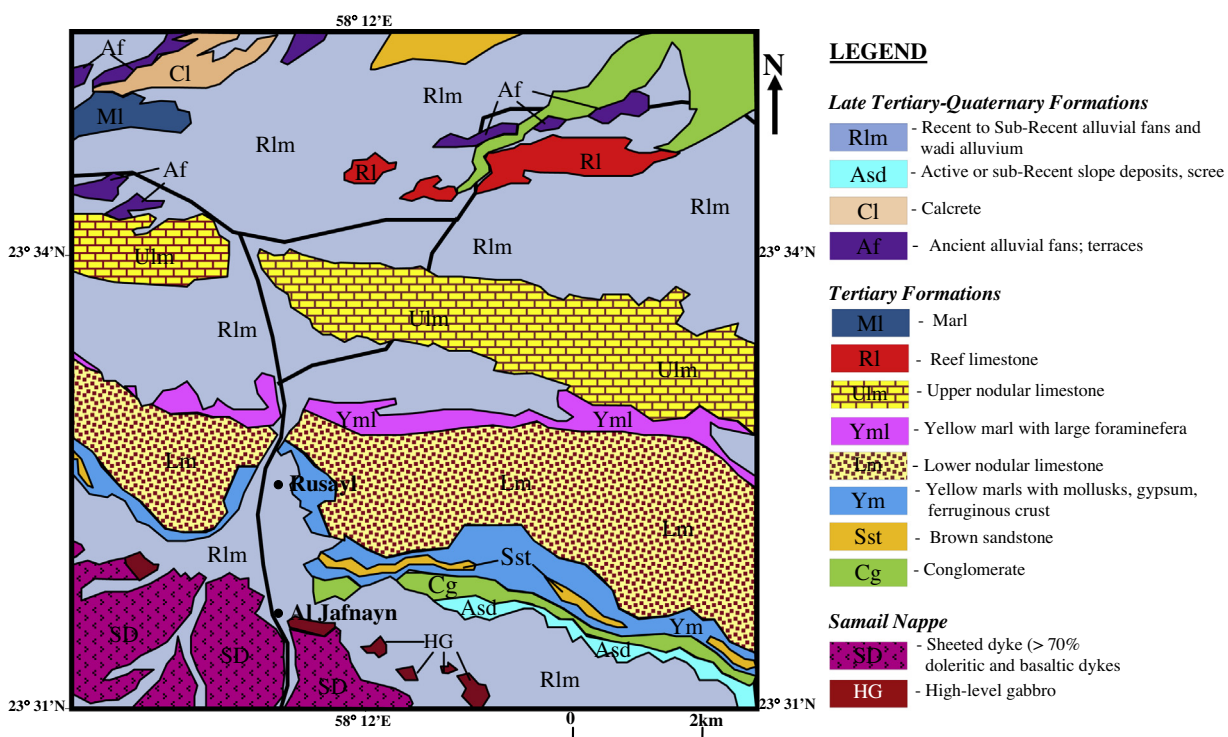


Fig. 2. Geological map of Rusayl and Al Jafnayn regions (modified from Ministry of Petroleum and Minerals, 1992a).

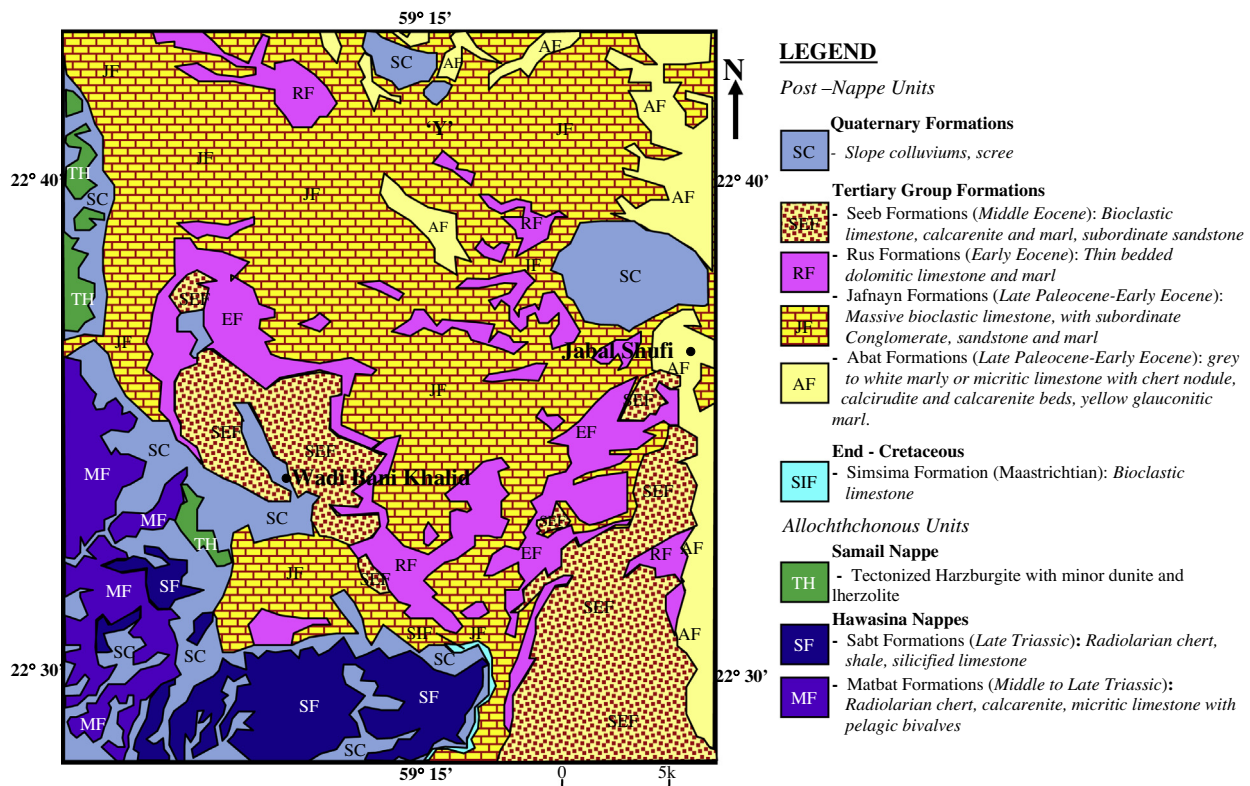


Fig. 3. Geological map of Site. 2 near to Sur region (modified from Ministry of Petroleum and Minerals, 1992b; after Rajendran and Nasir, 2013b).

unique occurrence of listwaenites and prospective hydrothermal mineralization in structures (Rajendran et al., 2013; Coffield, 1990, 1984; Glennie et al., 1973). Here, the listwaenites are associated with Parautochthon, Allochthon and Neoautochthon rock units. The bulk of the Parautochthon unit is composed of Hajar Supergroup. The Kahmah Group (Kh1, Kh2) of Late Jurassic to Lower Cretaceous age consists of pale grey silicified micritic limestone, massive blue limestone, conglomerate and yellow clayey limestone. The Kahmah Group is overlain by Muti Formation of Aruma Group which consists of siltstone and silty limestone. These Parautochthon Formations are overlain by Allochthonous units of Hawasina and Samail nappes. The chert is the lowest tectonic unit in the Allochthons in the Fanjah Saddle and crops out as discontinuous fault-bound slices around the flanks (Coffield, 1990). The major thrust plane separates the Muti Formation (Mu) and the overlying ophiolites where the hydrothermal altered listwaenites are occurred (Rajendran et al., 2013; Nasir et al., 2007). Considerable internal imbrications have disrupted and repeated the mélange and metamorphic sheets within the complex. The major rock types of the complex are siltstone, sandstone, radiolarian chert, olistoliths of reef limestone, the undifferentiated metamorphic rocks, meta-sediments and amphibolites. The basal portion of the ophiolite consists of serpentized harzburgite parallel to the sole thrust of the nappe. Above this the massive harzburgite and peridotite crops out below the cumulate gabbro. The sheeted dykes and extrusive basalts

are the highest units of the nappe (Coffield, 1990). The post-orogenic Autochthonous sedimentary rocks of the area are conglomerate (Cg), active or sub recent slope deposits, scree (Qgy) and sub-recent alluvial fans and terraces (Qgy-z) consists the yellow marly limestone, brown sandstone, clays, silts and recent alluvial sediments (Fig. 4).

2.4. Carbonatites of Musawi region

Carbonatites are alkaline ultramafic rock largely confined to the regions of lithospheric extension and associated with carbonatite magmatism (Nasir et al., 2011; Tappe et al., 2006, 2004; Le Roex and Lanyon, 1998). Along the northeastern margin of Oman, a strong extensional phase of alkaline magmatism (ultramafic lamprophyres, carbonatites, and sub volcanic intrusions) led to volcanic activity and seamount building is registered in the Batain basin during the break-up of Gondwana land around 160 Ma (Nasir et al., 2011; Hauser et al., 2001). The Musawi region (Site. 4; Figs. 1 and 5) is situated in the Batain basin mostly occurred with the late Permian Allochthonous units consist of Al Jil, Matbat, Wahrah, and Buwaydah Formations (Fig. 5; Nasir et al., 2011, Peters and Mercalli, 1998, Gnos et al., 1997; Meyer et al., 1996). Here, several ultramafic lamprophyric (aillikite and damtjernite) sill and dyke swarms and carbonatite bodies were identified (Nasir et al., 2011). The carbonatites are occurred within the Wahrah Formation which comprises a series of radiolarian cherts, shales and clay stones (Nasir et al., 2011). The

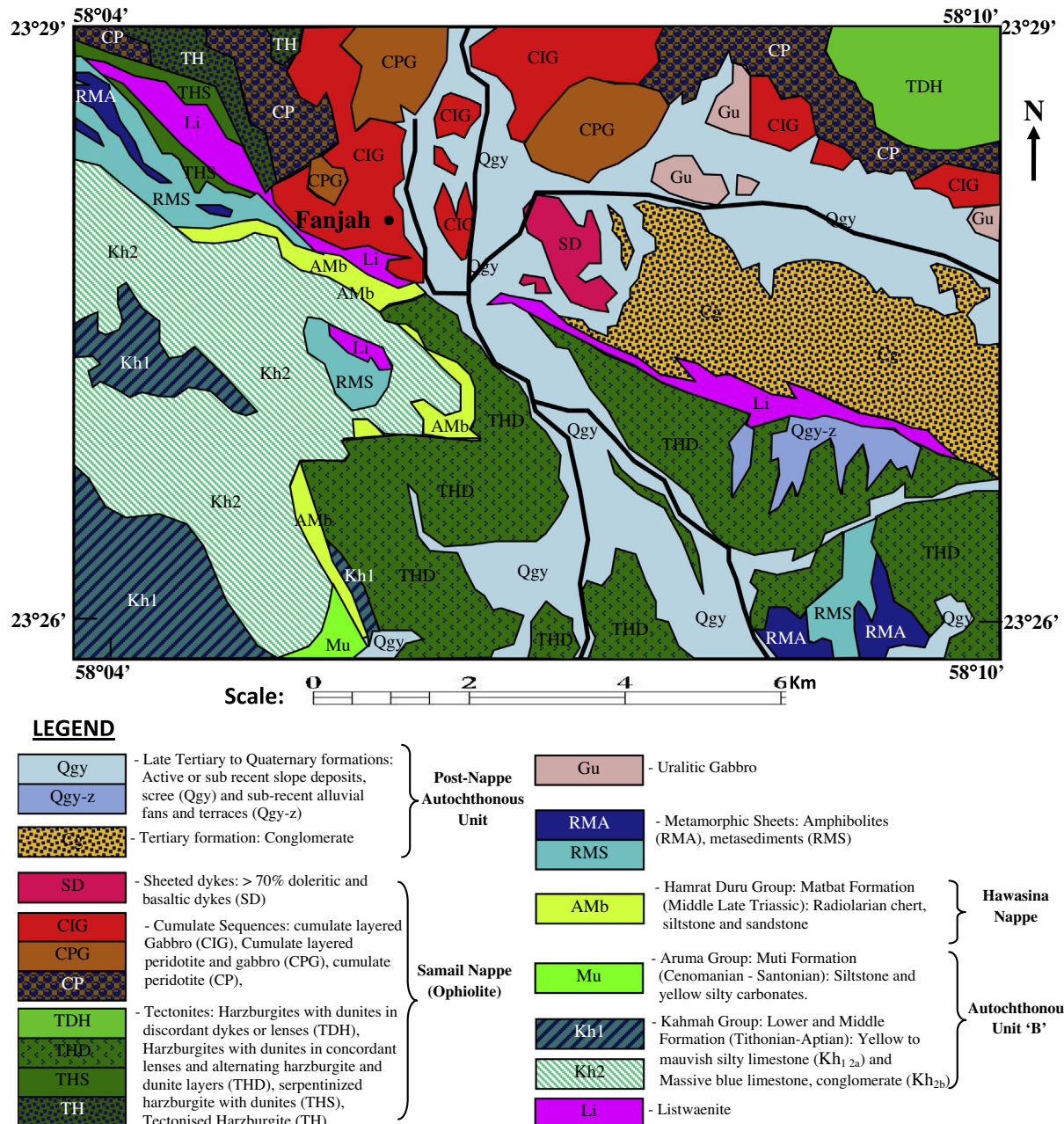


Fig. 4. Geological map in and around of Fanjah Saddle (modified from Ministry of Petroleum and Minerals, 1986; after Rajendran et al., 2013).

Allochthonous units are overlain by Post-nappe units. Though several exposures of carbonatites are found in this region, the study of spectral absorption of carbonatites is discussed on site 'X' (Fig. 5; Rajendran and Nasir, 2013a,b).

3. Satellite data and methods

ASTER data have been used widely by several workers to map silicate and carbonate rocks, as well as for volcanic studies (Rajendran and Nasir, 2013a,b; Rajendran et al., 2013, 2012, 2011a,b; Rowan and Mars, 2011; Gabr et al., 2010; Mars and Rowan, 2010; Amer et al., 2010; Ninomiya

et al., 2005). The ASTER sensor on board in the earth observing system (EOS) TERRA platform launched during December 1999 travels in a near circular, sun-synchronous orbit with an inclination of approximately 98.2°, an altitude of 705 km and a repeat cycle of 16 days offers relatively improved spatial, spectral, and temporal resolutions. It measures visible reflected radiation in three spectral bands (VNIR between 0.52 and 0.86 μm, with 15-m spatial resolution) and infrared reflected radiation in six spectral bands (SWIR between 1.6 and 2.43 μm, with 30-m spatial resolution). ASTER sensor records the data in band 3B (0.76–0.86 μm) with a backward looking angle that enables the calculation of Digital Elevation Models

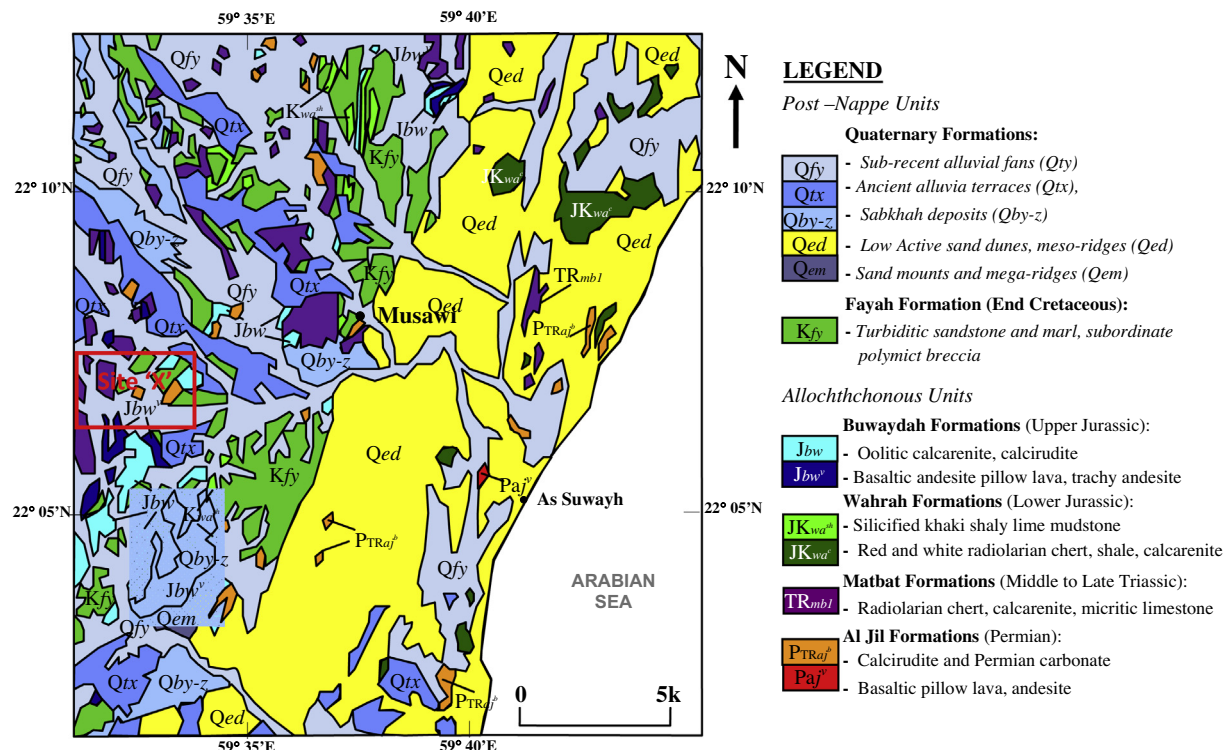


Fig. 5. Geological map of Musawi area (modified from Ministry of Petroleum and Minerals, 1992b; after Rajendran and Nasir, 2013a). 'X' is the region studied with ASTER satellite image.

(DEM). In addition, it receives emitted radiation in five spectral bands in the thermal infra-red region between 8.125 and 11.65 μm, with 90-m spatial resolution (Table 1; http://asterweb.jpl.nasa.gov/content/03_data/04_Documents/aster_user_guide_v2.pdf; Rajendran and Nasir, 2013a; Rajendran et al., 2012). The increase of spectral bands in the SWIR region (two spectral bands for Landsat vs. six spectral bands for ASTER) enhances the surface mineralogical and lithological mapping. In the present study, 14 ASTER Level 1B (L-1B) data of different sites were obtained from NASA Land Processes Distributed Active Archive Center User Services, USGS Earth Resources Observation and Science (EROS) Center (<https://LPDAAC.usgs.gov>; Table 2). The data were received in Tag Image File Format which provides files for each band containing the imagery and an ASCII text .met file containing the metadata. These were supplied in terms of scaled radiance at-sensor data with radiometric and geometric corrections applied. The imagery were

checked and found in cloud cover of 0% and for sensor errors, such as banding and other geometric distortions. The images were georeferenced in the UTM projection and WGS-84 ellipsoid datum. We chose the fourteen VNIR–SWIR–TIR spectral bands of the concerned study regions and processed to the sites of interest and interpreted to demonstrate the absorption characters of above discussed carbonate rocks using ENVI (4.8) and ArcGIS (10.1) software's. These have been evaluated by field checking and laboratory studies. The regional geological maps (Ministry of Petroleum and Minerals, 1986, 1992a,b) were used to verify the processed remote sensing data and occurrences of such carbonate rocks in field.

Systematic field works were carried out at several locations of four sites in different periods viz. September, 2012 and March, 2013 at Rusayl and Al Jafnayn regions; September and October 2011 at Fanjah region; August, 2012 at Sur Region and April 2012 and April 2013 at Musawi regions to evaluate the spectral study and verify

Table 1

Details of ASTER Level 1B data used in this study.

Site No.	Name of study sites	Date of acquisition of data	ASTER L1B data
Site. 1	Rusayl and Al Jafnayn region	March 29, 2004	AST_L1B_00303292004065157_20101106004827_15688
Site. 2	Region near Sur	April 07, 2004	AST_L1B_00304072004064549_20120220004813_10623
Site. 3	Fanjah region	March 29, 2004	AST_L1B_00303292004065157_20101106004827_15688
Site. 4	Musawi region	October 25, 2004	AST_L1B_00310252004063854_20111125105910_10652
Site chosen for validation of this study	Salalah region	November 30, 2001	AST_L1B_00311302001071009_20130912023704_19257

Table 2

Sensor characteristics of ASTER instruments.

Sensors	ASTER		
Characteristics	VNIR	SWIR	TIR
Spectral bands with range (μm)	Band 01 0.52–0.60 Nadir looking Band 02 0.63–0.69 Nadir looking Band 03N 0.76–0.86 Nadir looking Band 03B 0.76–0.86 Backward looking	Band 04 1.6–1.7 Band 05 2.145–2.185 Band 06 2.185–2.225 Band 07 2.235–2.285 Band 08 2.295–2.365 Band 09 2.36–2.43	Band 10 8.125–8.475 Band 11 8.475–8.825 Band 12 8.925–9.275 Band 13 10.25–10.95 Band 14 10.95–11.65
Spatial resolution (mm)	15	30	90
Swath width (km)	60	60	60
Radiometric resolution (bits)	8	8	12
Cross track pointing	$\pm 318 \text{ km} (\pm 24^\circ)$	$\pm 116 \text{ km} (\pm 8.55^\circ)$	$\pm 116 \text{ km} (\pm 8.55^\circ)$

the occurrence and distribution of carbonate minerals. During the field works, traverse based sample collection of minerals and rocks are carried out. The samples are used for spectral measurements, megascopic, microscopic, and minerals studies at the laboratory of Department of Earth Sciences, Sultan Qaboos University. The spectral properties of samples were studied by measuring the spectrum using a PIMA SP infrared spectrometer instrument which is fabricated for field spectroscopy by Integrated Spectronics Pty Ltd., Australia. It identifies and analyzes the spectral signal of minerals in the wavelength ranges from 1300 to 2500 nm with PIMA VIEW software (version 3.1). The spectral resolution of the device is $\sim 7 \text{ nm}$. It has a built in wavelength calibration target plate and is capable to measure spectra from 10 s to around 5 min speed. The application of this study is carried out on the limestone occurrences of part of Salalah region of Sultanate of Oman.

4. Spectral characters of carbonate minerals

Each mineral of earth surface has a unique response in interaction with electromagnetic radiation and creates a diagnostic spectral signature (Gupta, 2003; Clark, 1999) which conveys unique information related to the particular mineral. Several studies on minerals and rocks using absorption features of reflectance spectra in the spectral bands have been conducted by several authors (Van der Meer, 2004, 1995, 1994; Gupta, 2003; Clark, 1999; Gaffey, 1987, 1986, 1985; Crowley, 1986; Hunt, 1982, 1977; Hunt and Salisbury, 1971). Carbonate rocks are predominantly formed by calcite (CaCO_3) and dolomite ($\text{CaMg}(\text{CO}_3)_2$) minerals (compare to other type of carbonate minerals such as siderite (FeCO_3), magnesite (MgCO_3), aragonite (CaCO_3), ankerite $\text{CaFe}(\text{CO}_3)_2$, rhodochrosite (MnCO_3) etc.) in different proportion and have a diagnostic spectral absorption feature which can be used to distinguish each other (Van der Meer, 1995; Clark, 1999; Gaffey, 1987, 1986, 1985; Crowley, 1986; Hunt and Salisbury, 1971).

The earlier study on absorption features of carbonate minerals in the SWIR band (Van der Meer, 1994; Gaffey, 1987, 1986; Hunt and Salisbury, 1971; Huang and Kerr, 1960) shows a significant difference in the precise position of calcite and dolomite absorptions. Hunt and Salisbury (1971) found the calcite absorption centered at $2.35 \mu\text{m}$ and dolomite is at $2.33 \mu\text{m}$. Gaffey (1987, 1986) reported that the absorption of calcite is centered between 2.33 and $2.34 \mu\text{m}$ and dolomite is in between 2.31 and $2.32 \mu\text{m}$. In 1994, Van der Meer concluded that calcite absorption is centered at $2.3465 \mu\text{m}$ and dolomite is at $2.3039 \mu\text{m}$. Recent studies carried out by Rajendran et al. (2013), Rajendran and Nasir (2013a,b), Mars and Rowan (2010) and Combe et al. (2006) show that the calcite and dolomite (end members of series) can be distinguished and identified by variations in their absorptions between 2.33 and $2.45 \mu\text{m}$. The absorption features of reflectance spectra of calcite, dolomite, and aragonite in the range of wavelength between visible and SWIR is given in Fig. 6a (from Gaffey, 1986). Table 3 provides the position and width of absorption band of calcite and dolomite minerals in the SWIR (after: Gaffey, 1986) region. The work of Huang and Kerr (1960) indicates that calcite and dolomite have a strong absorption positions in the TIR at 11.40 and $11.35 \mu\text{m}$ respectively. Clark (1999) stated that the position of absorptions band of calcite and dolomite in the TIR are slightly shifted due to the different composition of the two minerals. Reig et al. (2002) has drawn attention to FTIR spectroscopy which showed that it could be used to determine absorption features of calcite at 875 cm^{-1} ($11.43 \mu\text{m}$) and 712 cm^{-1} ($14.04 \mu\text{m}$) and dolomite at 881 cm^{-1} ($11.35 \mu\text{m}$) and 730 cm^{-1} ($13.70 \mu\text{m}$). Fig. 6b shows the spectral absorption of calcite and dolomite minerals in TIR region (Clark, 1999).

5. ASTER sensitivity of carbonate rocks

ASTER sensor is characterized by diagnostic CO_3^2- absorption near 2.31 – $2.33 \mu\text{m}$ wavelengths in the ASTER

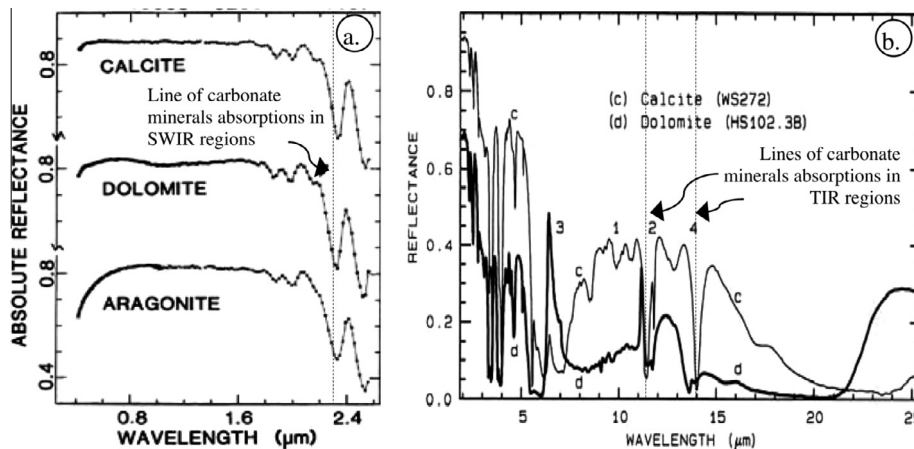


Fig. 6. The spectral absorptions of (a) calcite, dolomite, and aragonite in the visible to SWIR regions (Gaffey, 1986) and (b) calcite and dolomite in TIR region (Clark, 1999).

Table 3

The position and width of absorption band of calcite and dolomite in the SWIR region (after Gaffey, 1986).

Carbonate band	Calcite		Dolomite	
	Position (μm)	Width (μm)	Position (μm)	Width (μm)
1	2.530–2.541	0.0223–0.0255	2.503–2.518	0.0208–0.0228
2	2.333–2.340	0.0154–0.0168	2.312–2.332	0.0173–0.0201
3	2.254–2.720	0.0121–0.0149	2.234–2.248	0.0099–0.0138
4	2.167–2.179	0.0170–0.0288	2.150–2.170	0.0188–0.0310
5	1.974–1.995	0.0183–0.0330	1.971–1.979	0.0206–0.0341
6	1.871–1.885	0.0190–0.0246	1.853–1.882	0.0188–0.0261
7	1.753–1.885	0.0256–0.0430	1.735–1.740	0.0178–0.0395

spectral band 8 in SWIR region and 11.2 μm wavelengths in band 14 in TIR region to map carbonates minerals. The ASTER band 6 facilitates to map mica and clay minerals due to Al-OH absorption occurred near 2.20 μm wavelength. The ferric (Fe^{+3}) and ferrous (Fe^{+2}) irons absorptions are around 0.45 μm wavelength likely in ASTER band 1 and 1.0–1.1 μm wavelengths likely in ASTER band 3 which are helpful to discriminate iron rich weathered surface; and Si–O absorption near 8.7 μm wavelength in ASTER band 11 enables to study the presence of quartz and silicate minerals (Rajendran et al., 2011a; Mars and Rowan, 2010; Baldridge et al., 2009; Mars and Rowan, 2006; Ninomiya et al., 2005; Rowan et al., 1986). This is what makes ASTER sensor superior over other sensors for discrimination and mapping of different carbonate rocks. Based on the spectral absorption characters of such minerals, the minerals bearing rock types are discriminated using several image processing methods including false color composites (Harding et al., 1989), band ratios (Rajendran et al., 2013; Ninomiya et al., 2005; Sultan et al., 1987), decorrelation stretching (Rajendran and Nasir, 2013b; Philip et al., 2003; Abrams et al., 1988), and principal components analysis (Rajendran et al., 2013, 2012, 2011b; Khan et al., 2007).

The ASTER image spectra of major carbonate rocks of the regions in ASTER VNIR–SWIR (ASTER band 1 to

band 9 given in Fig. 7a) and ASTER TIR (ASTER band 10 to band 14 – represented as band 1 to band5 given in Fig. 7b) confirms their spectacular absorptions which are comparable to the spectra discussed in Fig. 6a and b. The spectra collected in VNIR–SWIR regions for limestones (collection of 12 sample points, Fig. 7a1) and marls (collection of 12 sample points, Fig. 7a2) show strong absorptions in ASTER spectral bands 3, 5 and 8. The absorption in band 3 is due to the presence of iron related informations; the absorption in band 5 characterizes the occurrences of altered minerals of the rock and in band 8 near 2.31–2.33 μm is due to the diagnostic absorption of CO_3 (Rajendran and Nasir, 2013b; Mars and Rowan, 2010; Abrams et al., 1988). The listwaenites exhibit absorptions (collection of 9 sample points, Fig. 7a3) in spectral bands 3, 5 and 7. The sharp absorption in band 7 in listwaenites is due to the presence of carbonates (classified as calcite-rich and dolomite-rich influenced with high Mn-oxide, Rajendran et al., 2013; Nasir et al., 2007). The carbonatites (collection of 8 sample points, Fig. 7a4) show absorptions in bands 3, 4 and 7. The absorption in band 4 is due to the occurrence of silicate minerals and the broad absorption in band 7 is due to the presence of carbonates and carbonate minerals in the carbonatites. The listwaenites and carbonatites can be distinguished in the band 7 based on the absorption feature and in the reflectance value which is rel-

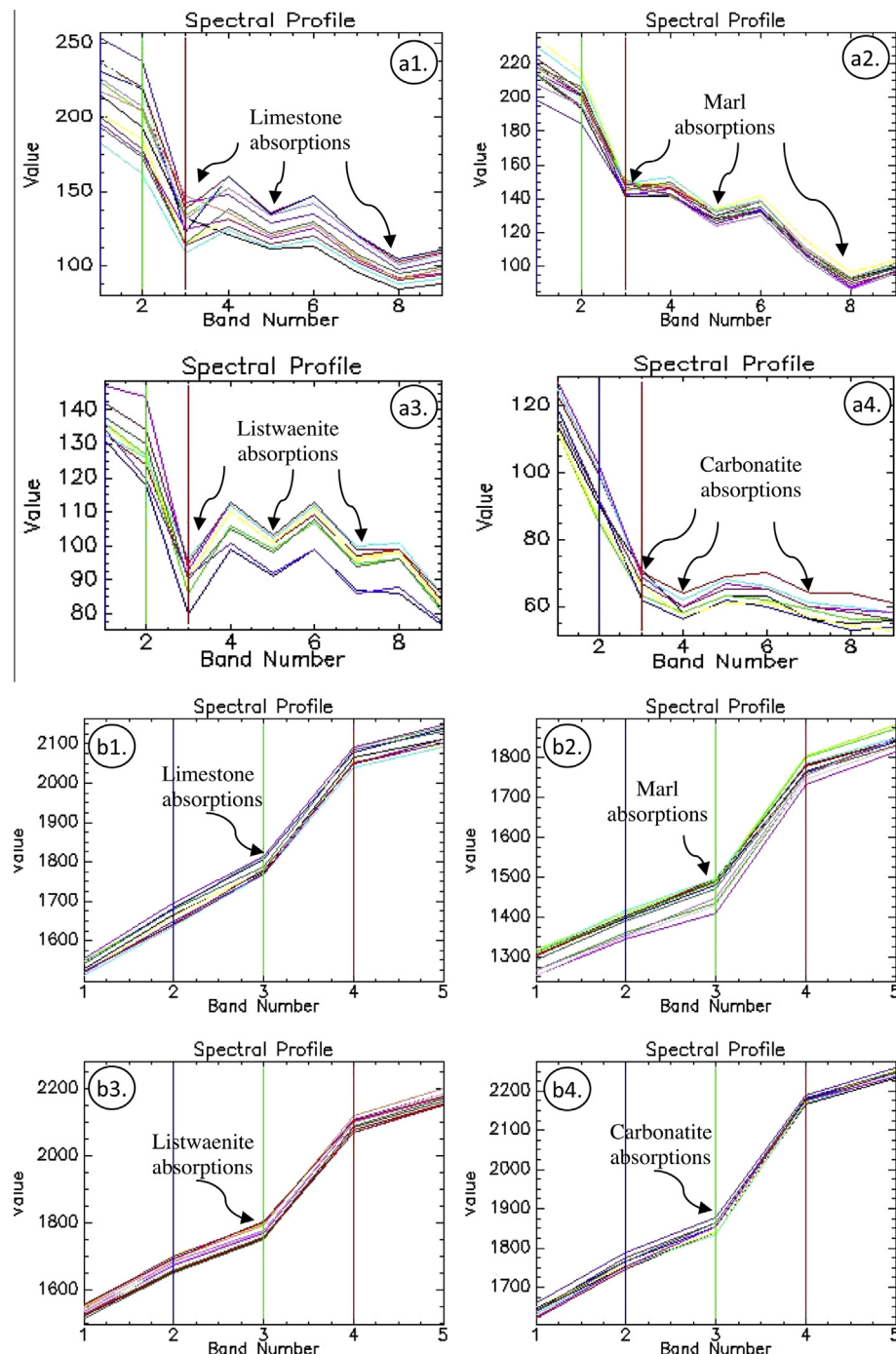


Fig. 7. ASTER image spectra of difference carbonate rocks of the study regions in VNIR-SWIR (a1–a4) and TIR (b1–b4) regions.

atively low in carbonatites compare to listwaenites due to presence of carbonates in the carbonatites. Thus, the four rocks are discriminated as carbonate rocks around the ASTER spectral band 8 based on the presence of the carbonate minerals that are predominantly occurred in these rocks. The ASTER band 5, distinguishes the limestones and marls (more hydroxyl clay minerals) due to the presence of altered minerals from listwaenite (hydrothermally altered rock) and carbonatites (ultramafic intrusive alkaline rocks which contain relatively more silicates detected in ASTER band 4).

The study on the intensity of the total absorptions against the reflections of these rocks in reflectance value axes shows the variations in intensity of absorptions. These are due to the variations in mineral compositions occurred in the surface of the rocks, which can be considered as an important reflectance parameters to distinguish these rocks and discriminate them in VNIR-SWIR regions. The limestones and marls (Fig. 7a1 and a2) show the intensity of total absorptions differences in between the values of 50–250 (in 'y' axis) whereas; the listwaenites and carbonatites (Fig. 7a3 and a4) show intensity differences in between 55

and 148 (in 'y' axis). The low intensity of absorptions (and high reflection values from 50 to 250) of limestones and marls compare to the high intensity of absorptions (and low reflection values from 55 to 148) of listwaenites and carbonatites are due to the presence of carbonate contents that occurred in different proportions in the limestones and marls. The high intensity of absorptions in listwaenites and carbonatites are due to the presence of Mn-oxide rich carbonates (calcite and dolomite) in listwaenites (Rajendran et al., 2013) and carbonates in carbonatites (Rajendran and Nasir, 2013a). It is also important to know that the carbonatites have high intensity of total absorption values compare to listwaenites, marls and limestones, which is due to the presence of total contents of carbonates (carbonates and carbonate minerals, Rajendran and Nasir, 2013a) that relatively high in carbonatites. This study not only distinguishes the carbonate rocks, but also classifies the rocks as sedimentary rocks (limestones and marls have low intensity of absorption or high reflection values), hydrothermal altered metamorphic rock (listwaenites have high intensity of absorption or low reflection values compare to sedimentary rock) and igneous rock (intrusive carbonatites have high intensity of absorptions compare to sedimentary and metamorphic rock in the high reflection values).

Furthermore, to distinguish the marls from limestone, listwaenite and carbonatites, we studied the ASTER image

spectra of all rock types in TIR region (Fig. 7b). The spectra collected over the same sample points that covers the points collected for ASTER VNIR–SWIR regions (Fig. 7a) shows the absorptions in TIR band 3 (ASTER band 12). The differences in emitted values are occurred around 1800 for limestones (collection of 8 sample points, Fig. 7b1), listwaenites (collection of 8 sample points, Fig. 7b3) and carbonatites (collection of 7 sample points, Fig. 7b4) except the marls (collection of 10 sample points, Fig. 7b2) which shows values around 1400. The low emitted value 1400 observed in marls (Fig. 7b2) among the rock types are due to the presence of hydroxyl bearing alumina-silicate minerals (clay minerals in marls) and H₂O-related features in the rock. The ASTER TIR spectral bands distinguishes the marls (have low emissivity of energy due to the presence of hydroxyl bearing alumina-silicate minerals) from the other rocks such as limestones, listwaenites and carbonatites (have high emissivity due to the absence of hydroxyl bearing alumina-silicate minerals and the presence of carbonate minerals and carbonates).

To demonstrate and confirm the spectral sensitivity characters of marls and carbonatites, the grey scale color images of 14 ASTER spectral bands of the study sites are provided in Figs. 8a and b (Rajendran and Nasir, 2013a,b). The grey scale image of marls (Site. 2; Fig. 8a) shows bright strong reflection in visible (0.4–0.7 μm) and

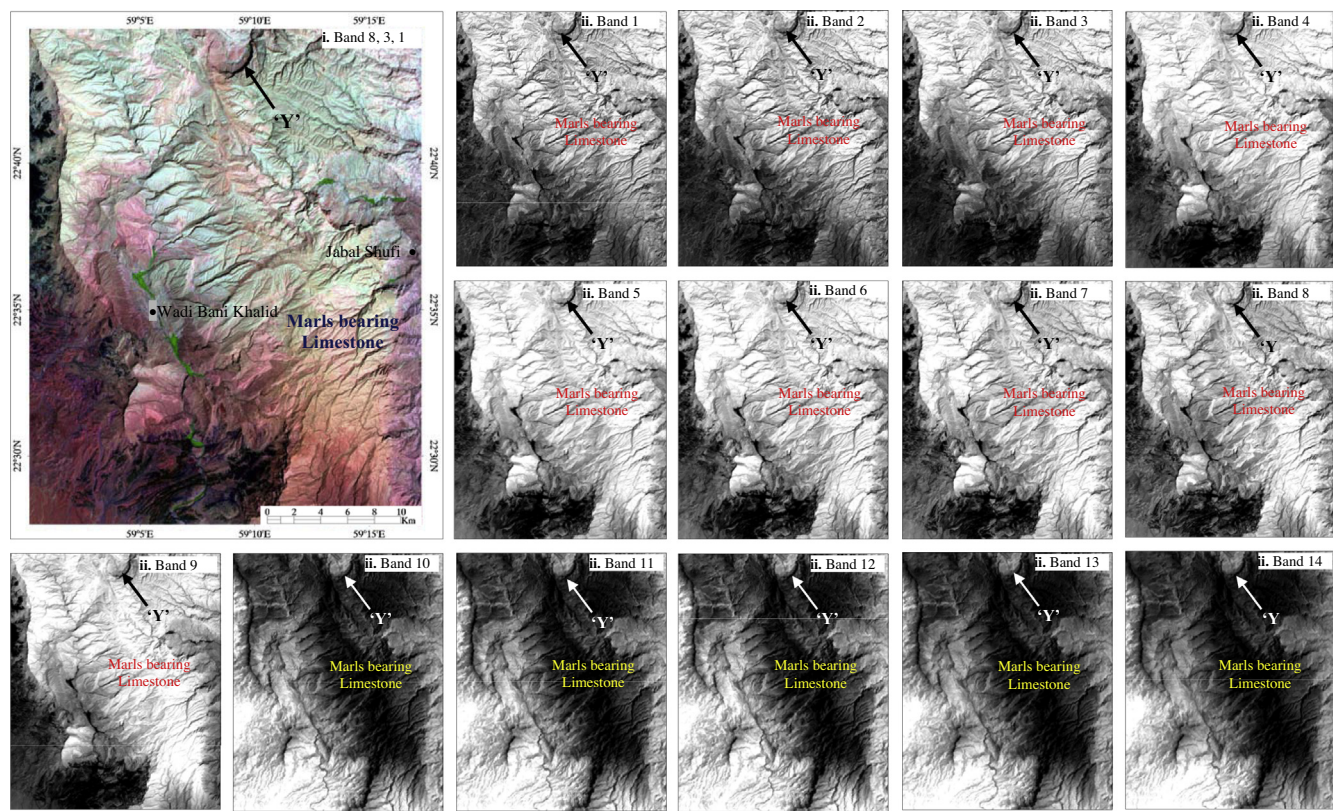


Fig. 8a. ASTER image of marls bearing limestone formations near Sur region (i) RGB (R:8; G:3; B:1) image and (ii). grey scale image show the marls bearing limestone formations in bright reflections in the visible and reflected infrared regions (band 1 to band 9) and dark absorptions in the TIR region (band 10 to band 14). 'Y' is the shadowed region.

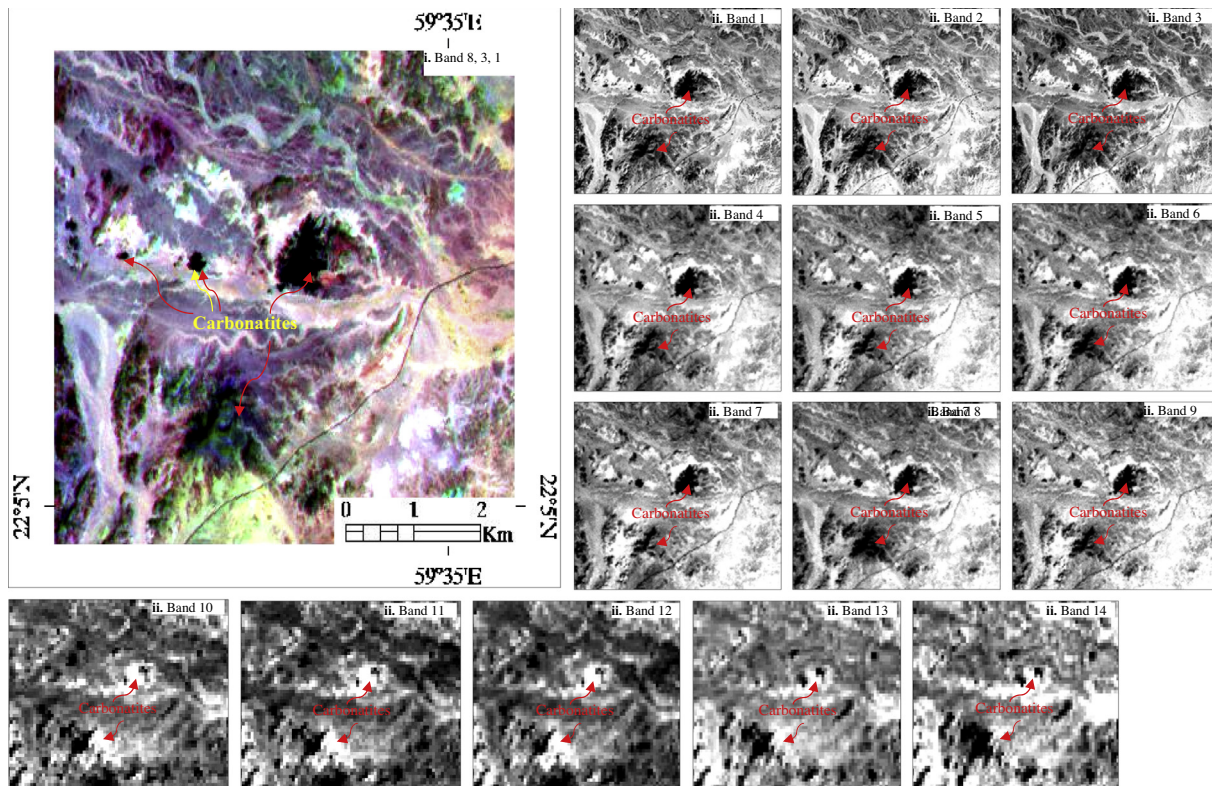


Fig. 8b. ASTER image of carbonatites occurrences near Musawi region (i) RGB (R:8; G:3; B:1 – carbonatites in black color) image and (ii) grey scale image show carbonatites in dark absorptions in the visible and reflected infrared regions (band 1 to band 9) and bright reflections in the TIR region (band 10 to band 14) (after Rajendran and Nasir, 2013a).

reflected infrared ($0.7\text{--}3\ \mu\text{m}$; includes the near IR $0.7\text{--}1.3\ \mu\text{m}$ and mid IR or SWIR $1.3\text{--}3\ \mu\text{m}$) spectral wavelength regions (Fig. 8a ii band 1 to band 9) due to the reflective characters of limestone bearing marl formations. The images (Fig. 8a ii band 10 to band 14) of TIR wavelength region ($3\text{--}14\ \mu\text{m}$) show strong dark absorptions due to the absorption of emitted energy by marls that consists altered hydroxyl bearing minerals occurred in and around of river flown (wadi) regions. The study and interpretation of shadowed region, that occurred due to steep slope and high relief at Site. 2 ('Y' in Fig. 8a; Google location: $22^{\circ}43'22.50''\text{N}$; $59^{\circ}9'29.70''\text{E}$) shows dark color in the entire ASTER VNIR-SWIR-TIR wavelength regions. This is due to the absence of energy absorption in the visible near infrared, shortwave infrared and energy emission in the thermal infrared wavelengths in the region. The study of water body occurred near to this study region shows dark in color in the entire ASTER VNIR-SWIR-TIR wavelength regions due to absorption of energy in the ASTER VNIR-SWIR regions and absence of emission of energy in the ASTER TIR region. Carbonatites of Site. 4 (Site. 'X' in Fig. 5 published in Rajendran and Nasir, 2013a) shows dark absorption throughout the entire wavelengths of visible and reflected infrared spectral wavelength regions (Fig. 8bii band 1 to band 9) due to absorption of incident energy and show bright color due to emission of energy in the entire wavelengths of thermal infrared

wavelength region (Fig. 8bii band 10 to band 14). The strong absorption of incident energy and high emission of energy are characterized by the presence of carbonates and carbonate minerals and absence of hydroxyl minerals in the carbonatites. These are verified in the field and confirmed through laboratory studies as discussed in the following Section 6. The ASTER spectral bands are capable in detecting the carbonate minerals (calcite and dolomite minerals occurred predominantly) and distinguishing the discussed rocks. The study proved that the remote sensing technique is capable in discriminating the rocks based on the spectral sensitivity of minerals.

6. Field and laboratory studies

In the field, the Tertiary Limestone Formations (Lm) of Late Paleocene to Early Eocene age of Jafnayn region (Site. 1, Figs. 1 and 2) crop out well in the Wadi Rusayl section and near to Rusayl village, west of Muscat, Oman. The formation consists of basal, nodular, crystalline limestones (Fig. 9a) with chert and ophiolite clasts. These are conformable and occurred above the marl and marly wackestone (Ym). It is interbedded by multicoloured shale, sandstone and conglomerate. The lower marly part formation consists of bivalve's gastropods and small corals. The upper boundary is conformable with the Rusayl Formation (Lower–Middle Eocene). The Rusayl Formation

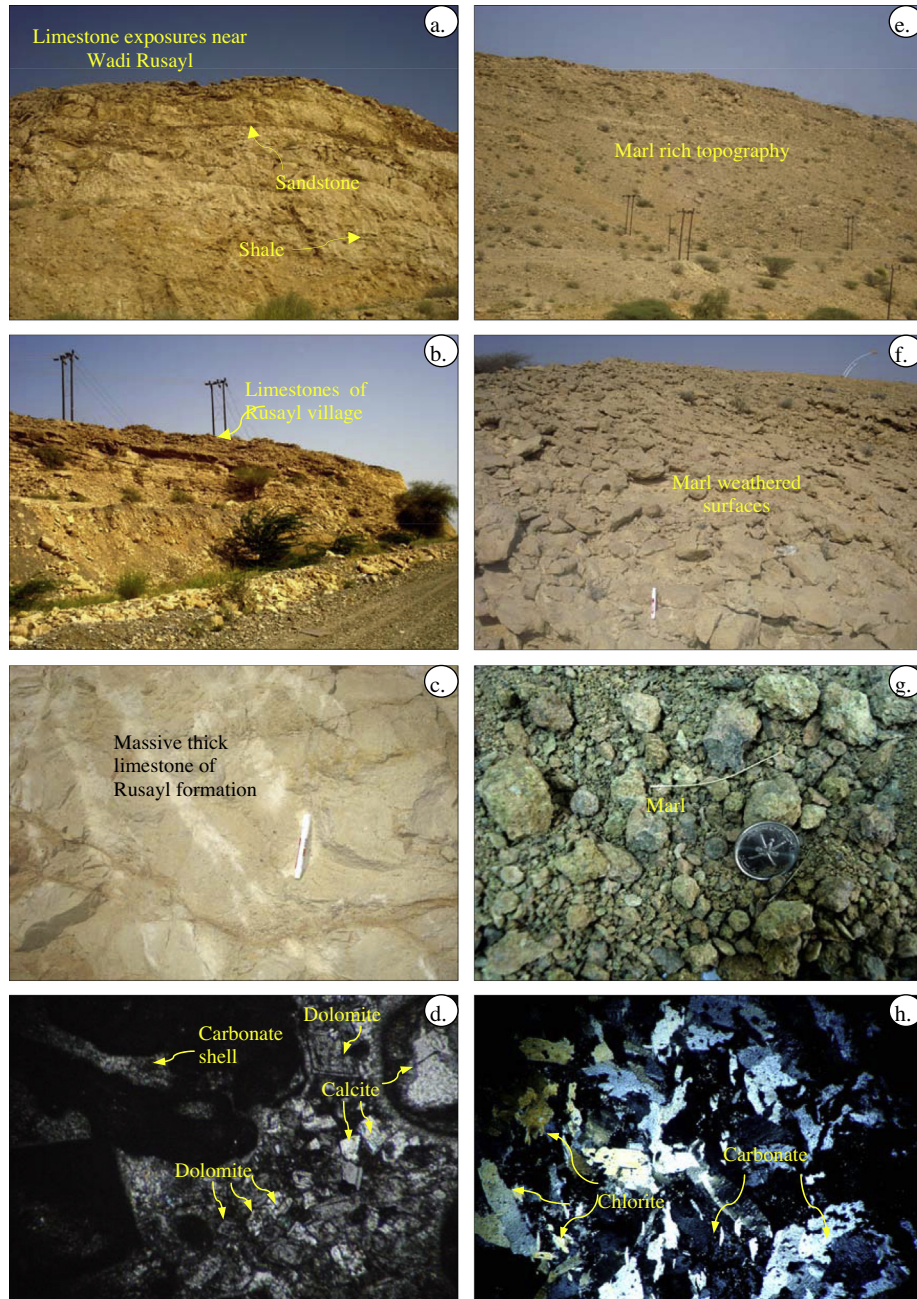


Fig. 9. Limestones of Al Jafnayn region in the field (a–c) and under the microscope (d, nicols crossed, 25×) and the marls bearing limestone of Sur region in the field (e–g) and under the microscope (h, nicols crossed, 25×).

(Ulm, Site. 1, Figs. 1 and 2) contains thick, resistant and nodular microcrystalline limestone followed soft multicolored shale and marl which consists shells and microspores (Fig. 9b and c). Exposures of shales and marls are characterized the formation and are all highly weathered. The basal unit consists of poorly indurated, multicolored shale and marl with occasional thin and microcrystalline limestones. The contact between the Rusayl and Jafnayn Formations is sharp. The major carbonate minerals namely calcite and dolomite occurred predominantly in the limestone which are observed under the microscope (Fig. 9d).

The Tertiary Group of Sur region (Site. 2) namely Abat, Jafnayn, Rus and Seeb Formations are horizontal in field and successively deposited. The marly limestones of Abat Formations are friable, white coloured occurred with chert nodule fragments. The marl in the limestone formations appears in yellow color. The formations are over lined by massive thick limestone formation consist of bioclast shells and interbedded with conglomerate and sandstone of Jafnayn Formations. Here, the marls are occurring as thin layers and rich in glauconite and chlorite minerals. The contact between the Abat and Jafnayn Formations are non-sequence. The Seeb Formations are occurred as cap

to Jafnayn Formation. The formations are thick and mainly consist of bioclastic limestone, sandstone and marl. These are underlain by Rus Formation consist of thin marl and dolomites. In field, the marls rich limestones are more friable (Fig. 9e and f) and are white in color. The interbedded marls are pale green in colour and rich in glauconite and clay minerals (Fig. 9g). The occurrences of minerals are confirmed under the microscope (Rajendran and Nasir, 2013b; Fig. 9h).

Listwaenites of Fanjah region are found at several locations and occurred as prominent hill (Fig. 10a) developed

within the dark green to black serpentinized harzburgite (tectonites part of the ophiolite association) in the hanging wall along the thrust fault. The rocks are altered and appear in dark brown to red and yellow in colors with porous textures (Fig. 10b). The colors are probably due to presence of iron, magnesium and manganese contents in the rocks. The listwaenites of the area are associated with metasediments and metamorphic amphibolites and shows alteration halos. In hand specimen, the rock shows the occurrences of carbonate minerals such as calcite and dolomite and can be classified as listwaenites rich in calcite and

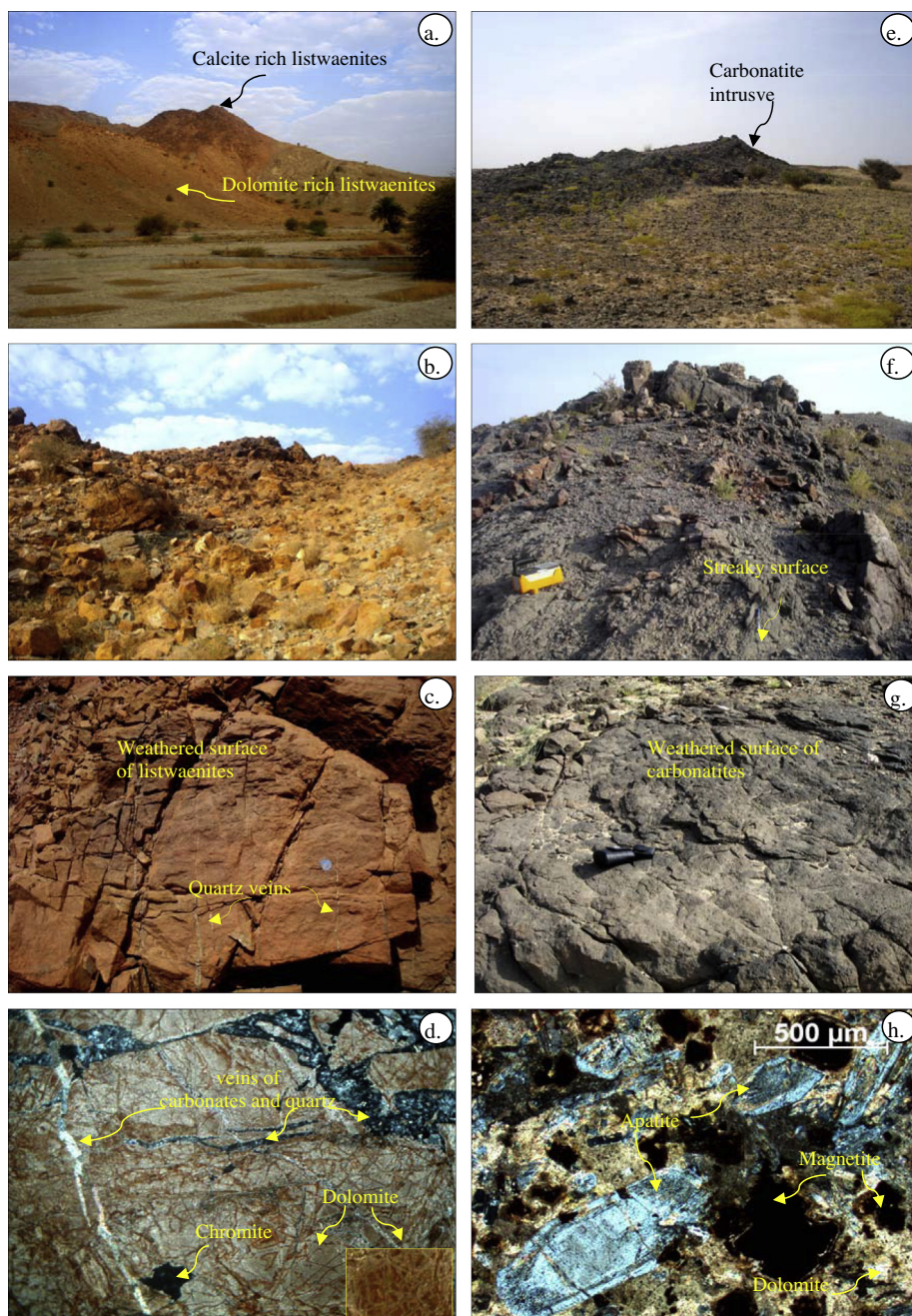


Fig. 10. Listwaenites of Fanjah region in the field (a–c) and under the microscope (d, nicks crossed, 35×, inset photo shows the euhedral dolomite) and the carbonatites of Musawi region in the field (e–g) and under the microscope (h).

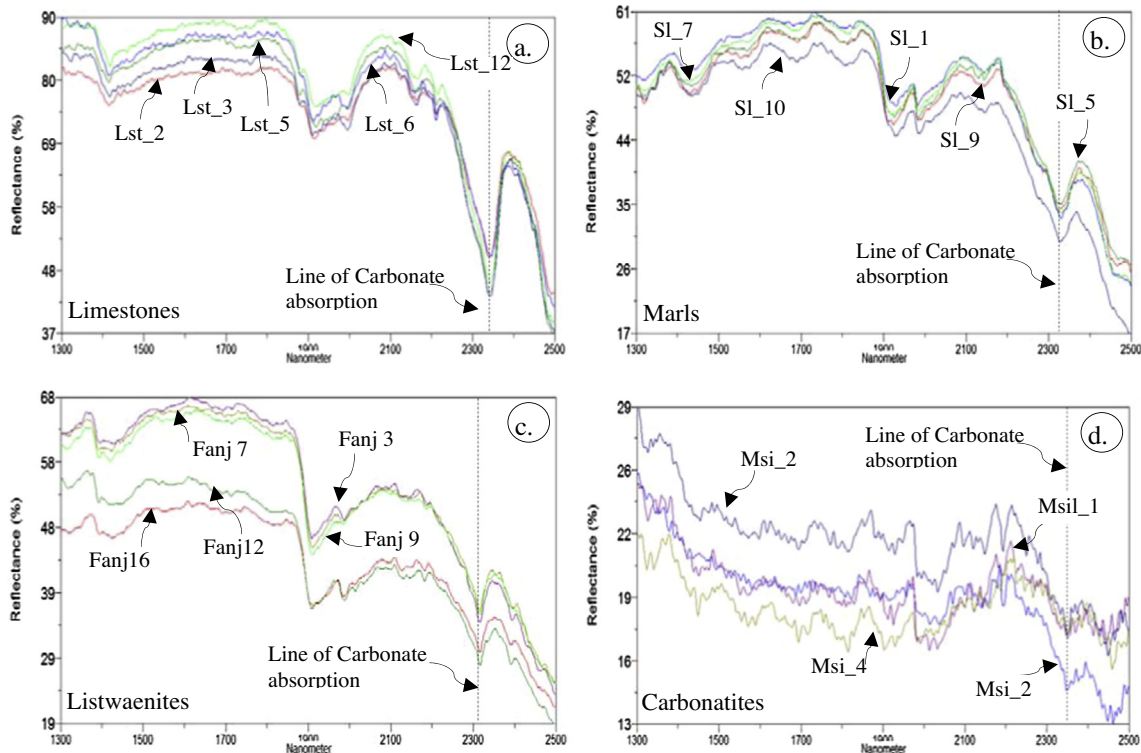


Fig. 11. Laboratory spectral plots of carbonate rocks (a) limestone of Rusayl and Al Jafnayn regions, (b) marls of Sur region, (c) listwaenites of Fanjah region and (d) carbonatites of Musawi region.

dolomite (Rajendran et al., 2013; Nasir et al., 2007). The rocks are occurred with micro and macro-crystalline quartz developed due to the removal of silica from serpentinites (Fig. 10c) during hydrothermal alteration (Rajendran et al., 2013). The microscopic thin section study of listwaenite shows that these are rich in dolomites occurred with chalcedony in fibers and small quartz crystals. The accessory minerals are chromite and magnetite (Fig. 10d).

The occurrence of carbonatites in Musawi regions are intrusive (Fig. 10e) within the Allochthonous radiolarian cherts of the Wahra Formation, which is surrounded by a well exposed sequence of sedimentary formations of post-nappe units and occurring in Batain plain parallel to the margin of the Oman coast. In the field, the rocks are massive, streaky and pyroclastically fluidal (Fig. 10f). These are strongly jointed and show weathered to a very rough surface with a crust of iron oxide (Fig. 10g). In hand specimens, the samples were light grey to dark brown in colour, fine-grained and porphyritic. Under the microscope, the carbonatites predominantly consist of dolomite and calcite and altered phlogopite minerals, with minor amounts of strontianite, REE-rich apatite, monazite, magnetite, spinel, zircon, and rutile. The abundance of ovoid patches are due to the occurrences of coarser-grained dolomite and euhedral prismatic phenocrysts of fluorapatite ranging from a few tens to 500 μm in length (Fig. 10h; Rajendran and Nasir, 2013a,b).

More than two hundred fifty spectral measurements have been taken using a PIMA SP infrared spectrometer at different locations in the field and over the samples

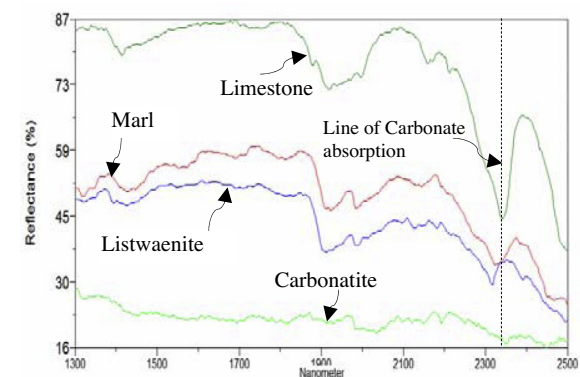


Fig. 12. Plot of selected spectra of different carbonate rocks show absorptions variations.

collected in the laboratory. The obtained spectral plots over the samples are well correlatable with the studied spectra (Figs. 6 and 7), which showed the spectral absorptions around 2.3 μm in all rock types (Fig. 11) due to the presence of major carbonate minerals namely calcite and dolomite in various percentages in these rocks. The hydroxyl mineral montmorillonite associated with carbonate minerals are also detected in the samples. The spectral plots of selected samples of limestones, marls, listwaenites and carbonatites are given in Fig. 11. The spectra of carbonatites collected over the samples in the laboratory show noisy due to the streaky surface of samples, however the line of absorption of carbonates is able to interpret from the plot.

Fig. 12 show the selected spectra of different rock types which also able to demonstrate the total intensity of absorptions against the reflectances. As discussed above, the laboratory spectra limestone show low intensity of absorptions (and high reflection values around 85) due to

the presence of carbonate contents that occurred in different proportions compare to carbonatites which have high intensity of absorptions (low reflection values around 25) due to the occurrence of carbonates and carbonate minerals in carbonatites.

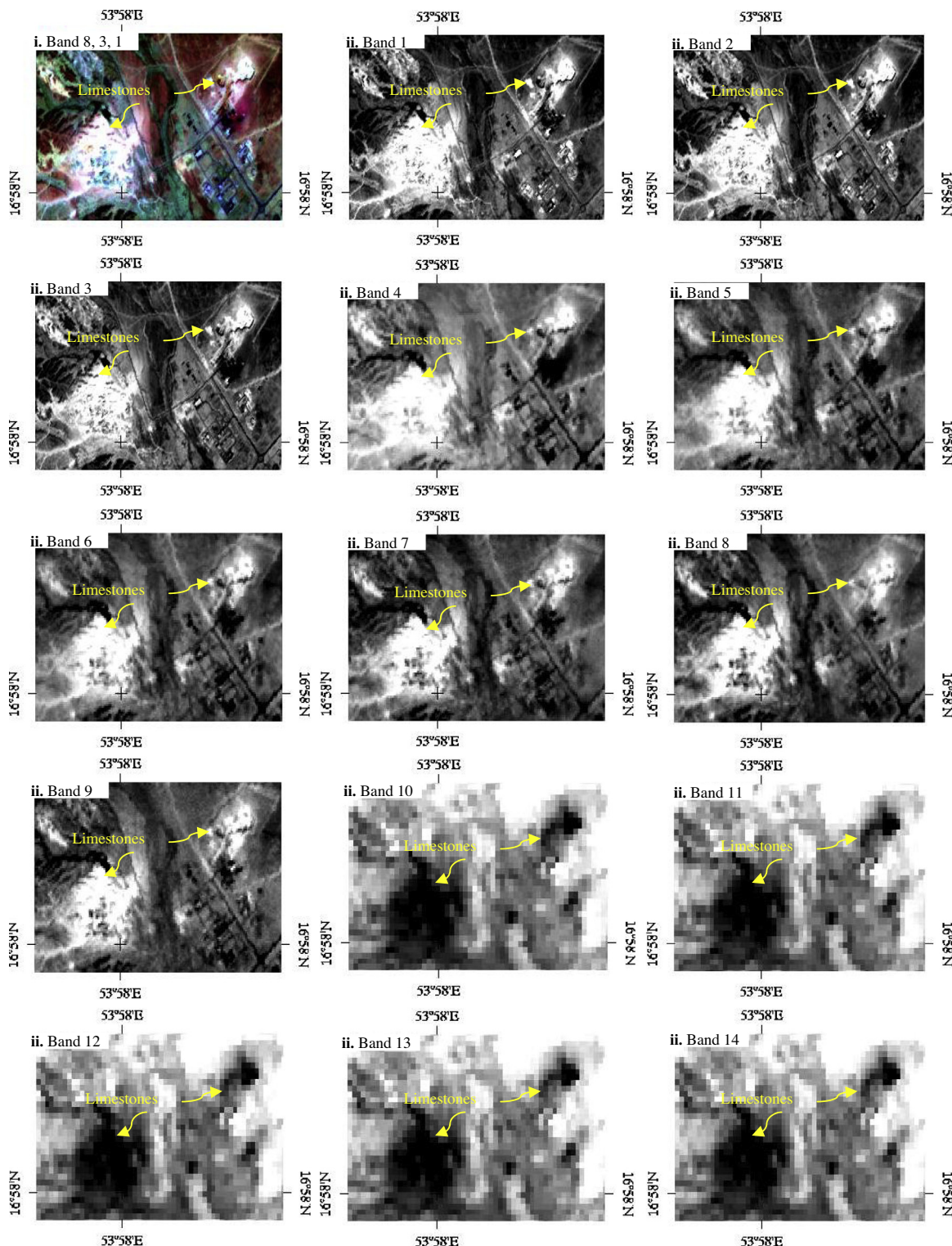


Fig. 13. ASTER image of limestone occurrences near Salalah region (i) RGB (R:8; G:3; B:1) image and (ii) grey scale image show limestones in bright reflections in the visible and reflected infrared regions (band 1 to band 9) and dark absorptions in the TIR region (band 10 to band 14).

7. Application of the study

The Sultanate of Oman has wide occurrences of carbonate deposits of Tertiary age. Two major industries viz. (1) Oman Cement Factory, near Rusayl (Google location: 23°29'31.67"N; 58°16'23.57"E) and (2) Global Mining Industry LLC., near Salalah (produces high grade limestone and gypsum, Google Location: 16°58'10.60"N; 53°57'36.51"E) are located in the region. Both are developed over the limestone deposits of Tertiary age. In this study, the limestone occurrences of Salalah region is considered as newer site to prove the spectral sensitivity of carbonate deposits and to show the ability of ASTER spectral bands for identification of carbonates. The output of the processed 14 ASTER spectral bands of the chosen region and the images are given in Fig. 13. The study and interpretation of the ASTER VNIR–SWIR images (Fig. 13ii band 1 to band 9) show clearly the occurrence of limestones in white colour due to the reflected energy of carbonate minerals of the limestones in the visible near infrared and short wave infrared wavelength regions. The images of ASTER TIR (Fig. 13ii band 10 to band 14) show strong dark absorptions due to the absorption of emitted energy by the minerals in the 3–14 μm wavelengths of thermal infrared region. Review of literatures show that the region is deposited with yellowish conglomerate limestone and bioclastic limestone belongs to Adawnib Formation of Fars Group of Tertiary age (Lepvrier et al., 2002). The ASTER spectral bands could able to identify the limestones of the region which show the potential of mapping carbonate formations. The methods and techniques studied are adoptable by the mining and exploration industries.

8. Conclusion

The present study describes and demonstrates the spectral absorption characters of economic important carbonate rocks namely limestone, marl, listwaenites and carbonatites occurred in parts of the Sultanate of Oman studying the spectral sensitivity carbonate minerals and bearing rocks by simple interpretation of image spectra collected over ASTER satellite data. The spectral absorption of carbonates, altered minerals and silicate minerals are described in ASTER VNIR–SWIR and TIR spectral bands and demonstrated by studying the grey color image. These have been verified in the field and studied in the laboratory. The study is time and cost-effective and the outcome may be useful to geologists and exploration communities looking carbonate rocks exploration. The technique is proved to be useful in the area of extremely rugged topography in the arid region, where there is difficulty in exhaustive sampling and conventional geological mapping.

Acknowledgements

The authors are thankful to NASA Land Processes Distributed Active Archive Center User Services, USGS Earth

Resources Observation and Science (EROS) Center (<https://LPDAAC.usgs.gov>) for providing the ASTER and Landsat TM data. The study is supported by Sultan Qaboos Internal grant IG/SCI/ETHS/12/02. Authors are very much thankful to the anonymous reviewers and editor of the journal for their valuable reviews and providing constructive comments and suggestions that have helped to present the work lucidly.

References

- Abrams, M.J., Rothery, D.A., Pontual, A., 1988. Mapping in the Oman ophiolite using enhanced landsat thematic mapper images. *Tectonophysics* 151, 387–401.
- Ahijado, A., Casillas, R., Nagy, G., Fernández, C., 2005. Sr-rich minerals in a carbonatite skarn, Fuerteventura, Canary Islands (Spain). *Mineral. Petrol.* 84, 107–127.
- Amer, R., Kusky, T.M., Ghulam, A., 2010. Lithological mapping in the central eastern desert of Egypt using ASTER data. *J. Afr. Earth Sci.* 56 (2–3), 75–82.
- Kunov1, Aagel, Tsintsov, Zdravko, Banushev, Banush, 2007. Listwaenite type wall-rock alterations in Bulgaria – peculiarities and gold ore perspectives. *Geosciences*, 75–77.
- Baldridge, A.M., Hook, S.J., Grove, C.I., Rivera, G., 2009. The ASTER spectral library version 2.0. *Remote Sens. Environ.* 113, 711–715.
- Beavington Penny, S.J., Wright, V.P., Racey, A., 2006. The middle Eocene Seeb formation of Oman: an investigation of a cyclicity, stratigraphic completeness and accumulation rates in shallow marine carbonate settings. *Sediment. Res.* 76, 1137–1161.
- Enton, Bedini, 2009. Mapping lithology of the Sarfartoq carbonatite complex, southern West Greenland, using HyMap imaging spectrometer data. *Remote Sens. Environ.* 113, 1208–1219.
- Borojević Šoštaric, S., Palinkaš, L.A., Topa, D., Spangenberg, J.E., Prochaska, W., 2011. Silver-base metal epithermal vein and listwaenite types of deposit Crnac, Rogozna Mts., Kosovo. Part I: Ore mineral geochemistry and sulfur isotope study. *Ore Geol. Rev.* 40, 65–80.
- Clark, R.N., 1999. Spectroscopy of rock and minerals and principles of spectroscopy. In: Rencz, A.N. (Ed.), *Remote Sensing for the Earth Sciences: Manual of Remote Sensing*, vol. 3. John Wiley & Sons, New York, pp. 3–58, thired ed.
- Coffield, D.Q., 1984. Culmination collapse in the Fanjah saddle. *Oman (Abstract): Am. Assoc. Petrol. Geol. Bull.* 68, 463.
- Coffield, D.Q., 1990. Structures Associated with Nappe Emplacement and Culmination Collapse in the Central Oman Mountains, The Geology and Tectonics of the Oman Region, Special publication 49, The Geological Society, London, pp. 447–458.
- Combe, J.P., Launeau, P., Pinet, P., Despan, D., Harris, E., Ceuleneer, G., Sotin, C., 2006. Mapping of an ophiolite complex by high-resolution visible-infrared spectrometry. *Geochem. Geophys. Geosyst.* 7 (8), 1–11.
- Crowley, J.K., 1986. Visible and near-infrared spectra of carbonate rocks: reflectance variations related to petrographic texture and impurities. *J. Geophys. Res.* 91 (B5), 5001–5012.
- David, I.G., Noreen, M.V., 2001. The Phalabowra (Palabora) carbonatite-hosted magnetite–copper sulphide deposit, South Africa: an end-member of the iron-oxide copper–gold–rare earth element deposit group?. *Miner. Deposita* 36 189–194.
- Gabr, S., Ghulam, A., Kusky, T., 2010. Detecting areas of high-potential gold mineralization using ASTER data. *Ore Deposit Rev.* 38, 59–69.
- Gaffey, S.J., 1985. Reflectance spectroscopy in the visible and near infrared (0.35–2.55 microns): applications in carbonate petrology. *Geology* 13, 270–273.
- Gaffey, S.J., 1986. Spectral reflectance of carbonate minerals in the visible and near infrared (0.35–2.55 microns): calcite, aragonite, and dolomite. *Am. Mineral.* 71, 151–162.

- Gaffey, S.J., 1987. Spectral reflectance of carbonate minerals in the visible and near infrared (0.35–2.55 microns): anhydrous carbonate minerals. *J. Geophys. Res.* 92 (B2), 1429–1440.
- Glennie, K.W., Boeuf, M.G.A., Hughes Clarke, M.W., Moody-Stuart, M., Pilaar, W.F.H., Reinhardt, B.M., 1973. Late cretaceous nappes in the Oman Mountains and their geologic significance. *Am. Assoc. Petrol. Geol. Bull.* 57, 5–27.
- Gnos, E., Immenhauser, A., Peters, T., 1997. Late cretaceous early tertiary convergence between the Indian and Arabian plates recorded in ophiolites and related sediments. *Tectonophysics* 271, 1–19.
- Groves, I.G., Vielreicher, N.M., 2001. The Phalabowra (Palabora) carbonatites-hosted magnetite–copper sulphide deposit, south Africa: an end-member of the iron-oxide copper–gold–rare earth element deposit group? *Mineral. Deposita* 36, 189–194.
- Gupta, R.P., 2003. *Remote Sensing Geology*, second ed. Springer, Heidelberg.
- Hamilton, W.R., Woolley, A.R., Bishop, A.C., 1995. Hamlyn Guide: Minerals, Rocks and Fossils, Mandarin Offset, Hong Kong.
- Harding, D.J., Wirth, K.R., Bird, J.M., 1989. Spectral mapping of Alaskan ophiolites using landsat thematic mapper data. *Remote Sens. Environ.* 28, 219–232.
- Hauser, M., Martini, R., Burns, S., Dumitrica, P., Kristyn, L., Matter, A., Peters, T., Zaninetti, L., 2001. Triassic stratigraphic evolution of the Arabian–Greater India embayment of the southern Tethys margin. *Econ. Geol.* 94, 29–62.
- http://asterweb.jpl.nasa.gov/content/03_data/04_Documents/aster_user_guide_v2.pdf.
- Huang, C.K., Kerr, P.F., 1960. Infrared study of the carbonate minerals. *Am. Mineral.* 45, 311–324.
- Hughes Clarke, M.W., 1988. Stratigraphy and rock unit nomenclature in the oil producing area of interior Oman. *Petrol. Geol.* 11, 5–60.
- Hunt, G.R., Salisbury, J.W., 1971. Visible and near infrared spectra of minerals and rocks: II. Carbonates. *Mod. Geol.* 2, 23–30.
- Hunt, G.R., 1977. Spectral signatures of particulate minerals in the visible and near infrared. *Geophysics* 42, 501–513.
- Hunt, G.R., 1982. Spectroscopic properties of rocks and minerals. In: Carmichael, R.S. (Ed.), *Handbook of Physical Properties of Rock*, vol. I. CRC Press, Boca Raton, pp. 295–385.
- Jones, B., Desrochers, A., 1992. Shallow platform carbonates. In: Walker, R.G., James, N.P. (Eds.), *Facies Models: Response to sea level changes*, Geological Association of Canada, 227–301.
- Kervyn, M., Ernst, G.G.J., Harris, A.J.L., Belton, F., Mbede, E., Jacobs, P., 2008. Thermal remote sensing of the low-intensity carbonatites volcanism of Oldoinyo Lengai, Tanzania. *Int. J. Remote Sens.* 29 (22), 6467–6499.
- Khan, S.D., Mahmood, K., Casey, J.F., 2007. Mapping of Muslim Bagh ophiolite (Pakistan) using new remote sensing and field data. *J Asian Earth Sci.* 30, 333–343.
- Kuleshevich, L.V., 1984. Listvenites in the greenstone belts of Eastern Karelia. (*Geologiya Rudnykh Mestorozhdenii*) *Geol. Ore Deposits* 3, 112–116.
- Leblanc, M., Fischer, W., 1990. Gold and platinum group elements in cobalt-arsenide ores: hydrothermal concentration from a serpentinite source-rock (Bou Azzer, Morocco). *Mineral. Petrol.* 42, 197–209.
- Lepvrier, C., Fournier, M., Bérard, T., Roger, J., 2002. Cenozoic extension in coastal Dhofar (southern Oman): implications on the oblique rifting of the Gulf of Aden. *Tectonophysics* 357, 279–293.
- Le Roex, A.P., Lanyon, R., 1998. Isotope and trace element geochemistry of Cretaceous Damaral and lamprophyres and carbonatites, northwestern Namibia: evidence for plume–lithosphere interactions. *J. Petrol.* 39, 1117–1146.
- Madani, A., Harbi, H., Eldougoudou, A., 2008. Utilization of remote sensing techniques for mapping the listwaenite associated with Jabal Al-Wask Ophiolite Complex, Northwestern Saudi Arabia. *Egypt. J. Remote Sens. Space Sci.* 11, 57–72.
- Mars, J.C., Rowan, L.C., 2006. Regional mapping of phyllitic- and argillic-altered rocks in the Zagros magmatic arc, Iran, using advanced spaceborne thermal emission and reflection radiometer (ASTER) data and logical operator algorithms. *Geosphere* 2 (3), 161–186.
- Mars, J.C., Rowan, L.C., 2010. Spectral assessment of new ASTER SWIR surface reflectance data products for spectroscopic mapping of rocks and minerals. *Remote Sens. Environ.* 114, 2011–2025.
- Meyer, J., Mercoulli, I., Immenhauser, A., 1996. Off ridge alkaline magmatism and seamount volcanoes in the Masirah Island ophiolite, Oman. *Tectonophysics* 267, 187–208.
- Ministry of Petroleum and Minerals, 1992a. Geological Map, Oman (1:250,000). SEEB Sheet NF 40–03.
- Ministry of Petroleum and Minerals, 1992b. Geological Map, Oman (1:250,000) Sur Sheet NF40-08.
- Ministry of Petroleum and Minerals, 1986. Geological Map, Oman (1:100,000) Fanjah Sheet NF40-3F.
- Mitchell, R.H., 2005. Carbonatites and carbonatites and carbonatites. *Can. Mineral.* 43, 2049–2068.
- Nasir, S., Al-Khirbashi, S., Rollinson, H., Al-Harthy, A., Al-Sayigh, A., Al-Lazki, A., Theye, T., Massonne, H.J., Belousova, E., 2011. Petrogenesis of early cretaceous carbonatite and ultramafic lamprophyres in a diatreme in the Batain Nappes, Eastern Oman continental margin. *Contrib. Mineral. Petrol.* 161, 47–74.
- Nasir, S., Theye, T., Massonne, H.J., 2009. REE-rich aeschynite in apatite-dolomite carbonatite, Eastern Oman Mountains. *Open Mineral. J.* 3, 17–27.
- Nasir, S., Al Sayigh, A., Al Harthy, A., Al-Khirbashi, S., Al-Jaaidi, O., Musllam, A., Al-Mishwati, A., Al-Bu'saidi, S., 2007. Mineralogical and geochemical characterization of listwaenite from the Semail Ophiolite, Oman. *Chmie der Erde – Geochem.* 67 (3), 213–228.
- Ninomiya, Y., 2002. Mapping quartz, carbonate minerals and mafic–ultramafic rocks using remotely sensed multispectral thermal infrared ASTER data. *P SPIE* 4710, 191–202.
- Ninomiya, Y., Fu, B., Cudahy, T.J., 2005. Detecting lithology with advanced spaceborne thermal emission and reflection radiometer (ASTER) multispectral thermal infrared “radiance-at-sensor” data. *Remote Sens. Environ.* 99, 127–139.
- Peters, T., Mercalli, I., 1998. Extremely thin oceanic crust in the Proto-Indian Ocean: evidence from the Masirah Ophiolite, Sultanate of Oman. *J. Geophys. Res. Solid Earth* 103, 677–689.
- Pettijohn, F.J., 1957. *Sedimentary Rocks*. Harper & Brothers, New York, p. 4103.
- Philip, G., Ravindran, K.V., Mathew, J., 2003. Mapping the Nidar ophiolite complex of the Indus suture zone, Northwestern-Trans Himalaya using IRS-1C/1D data. *Int. J. Remote Sens.* 24, 4979–4994.
- Racey, A., 2001. A review of Eocene Nummulite accumulations: structure, formation and reservoir potential. *Petrol. Geol.* 24 (1), 79–100.
- Rajendran, S., Nasir, S., Kusky, T.M., Ghulam, A., Gabr, S., El Gali, M., 2013. Detection of hydrothermal mineralized zones associated with listwaenites rocks in the Central Oman using ASTER data. *Ore Geol. Rev.* 53, 470–488.
- Rajendran, S., Nasir, S., 2013a. ASTER spectral analysis of ultramafic lamprophyres (carbonatites and aillikites) within the Batain nappe, northeastern margin of Oman – a proposal developed for spectral absorption. *Int. J. Remote Sens.* 34 (8), 2763–2795.
- Rajendran, S., Nasir, S., 2013b. ASTER mapping of limestone formations and study of caves, springs and depressions in parts of Sultanate of Oman. *Environ. Earth Sci.* <http://dx.doi.org/10.1007/s12665-013-2419-7>.
- Rajendran, S., Al-Khirbashi, S., Pracejus, B., Nasir, S., Al-Abri, A.H., Kusky, T.M., Ghulam, A., 2012. ASTER detection of chromite bearing mineralized zones in semial ophiolite massifs of the northern Oman mountain: exploration strategy. *Ore Geol. Rev.* 44, 121–135.
- Rajendran, S., Hersi, O.S., Al-Harthy, A.R., Al-Wardi, M., Ali El-Ghali, M., Al-Abri, A.H., 2011a. Capability of advanced spaceborne thermal emission and reflection radiometer (ASTER) on discrimination of carbonates and associated rocks and mineral identification of Eastern Mountain region (Saih Hatat Window) of Sultanate of Oman. *Carbonates Evaporites* 26, 351–364.

- Rajendran, S., Thirunavukkarasu, A., Balamurugan, G., Shankar, K., 2011b. Discrimination of iron ore deposits of granulite terrain of Southern Peninsular India using ASTER data. *J. Asian Earth Sci.* 41, 99–106.
- Reig, F.B., Adelantado, J.V.G., Moya Moreno, M.C.M., 2002. FTIR quantitative analysis of calcium carbonate (calcite) and silica (quartz) mixtures using the constant ratio method. Application to geological samples. *Talanta* 58 (4), 811–821.
- Robertson, A.H.F., Searle, M.P., Ries, A.C., 1990. The Geology and Tectonics of the Oman Region, Edited volume Special publication 49, The Geological Society, London, pp. 1–845.
- Robertson A.H.F., Searle, M.P., 1990. The Northern Oman Tethyan Continental Margin: Stratigraphy, Structure, Concepts and Controversies, The Geology and Tectonics of the Oman Region, Special publication 49, The Geological Society, London, pp. 3–25.
- Rowan, L.C., Mars, J.C., 2003. Lithologic MAPPING in the Mountain Pass Area, California using advanced spaceborne thermal emission and reflection radiometer (ASTER) data. *Remote Sens. Environ.* 84, 350–366.
- Rowan, L.C., Mars, J.C., 2011. ASTER spectral analysis and lithologic mapping of the Khanneshin carbonatite volcano, Afghanistan. *Geosphere* 7, 276–289.
- Rowan, L.C., Kingston, M.J., Crowley, J.K., 1986. Spectral reflectance of carbonatite and related alkalic igneous rocks from four North American localities. *Econ. Geol.* 81, 857–871.
- Sherlock, R.L., Logan, M.A.V., 1995. Silica-carbonate alteration of serpentinite, implications for the association of mercury and gold mineralization in northern California. *Explor. Min. Geol.* 4, 395–409.
- Sultan, M., Arvidson, R.E., Sturchio, N.C., Guinness, E.A., 1987. Lithologic mapping in arid regions with landsat thematic mapper data: Meatiq dome, Egypt. *Geol. Soc. Am. Bull.* 99, 748–762.
- Tappe, S., Steenfelt, A., Heaman, L., Simonetti, A., 2009. The newly discovered Jurassic Tikiusaaq carbonatite-aillikite occurrence, West Greenland, and some remarks on carbonatites-kimberlite relationships. *Lithos* 112, 385–399.
- Tappe, S., Foley, S.F., Jenner, G.A., Heaman, L.M., Kjarsgaard, A.B., Romer, R.I., Stracke, A., Joyce, N.J., Hoefs, J., 2006. Genesis of ultramafic lamprophyres and carbonatites at Aillik Bay, Labrador: a consequence of incipient Lithospheric thinning beneath the North Atlantic Craton. *J. Petrol.* 47, 1261–1315.
- Tappe, S., Jenner, G.A., Foley, S.F., Heaman, L.M., Besserer, D., Kjarsgaard, B.A., Ryan, A.B., 2004. Torngat ultramafic lamprophyres and their relation to the North Atlantic alkaline province. *Lithos* 76, 491–518.
- Tsikouras, B., Karapi, S., Grammatikopoulos, A.T., Hatzipanagiotou, K., 2006. Listwaenite evolution in the ophiolite mélange of Iti Mountain. *Eur. J. Mineral.* 18, 243–255.
- Uçurum, A., 1998. Application of the correspondence-type geostatistical analysis on the Co, Ni, As, Ag and Au concentrations of the listwaenites from serpentinites in the Divriği and Kuluncak Ophiolitic Mélanges. *Turkish J. Earth Sci.* 7, 87–95.
- Uçurum, A., Larson, L.T., 1999. Geology, base precious metal concentration and genesis of the silica-carbonate alteration (listwaenites) from Late Cretaceous ophiolitic melanges at Cürek-Divriği in Sivas province and at Güvenç, Karakuz Hekimhan in Malatya province, Central East Turkey. *Chem. Erde Geochem.* 59, 77–104.
- Van der Meer, F., 1994. Sequential indicator conditional simulation and indicator kriging applied to discrimination of dolomitization in GER 63-channel imaging spectrometer data. *Nonrenewable Resour.* 3, 146–164.
- Van der Meer, F., 1995. Spectral reflectance of carbonate mineral mixtures and bidirectional reflectance theory: quantitative analysis techniques for application in remote sensing. *Remote Sens. Rev.* 13, 67–94.
- Van der Meer, F., 2004. Analysis of spectral absorption features in hyperpectral imagery. *Int. J. Appl. Earth Obs. Geoinf.* 5, 55–68.
- Wall, Frances., Mariano, A.N., 1996. Rare earth minerals in carbonatites—a discussion centered on the Kangankunde carbonatite, Malawi, in: Jones, A.P., Wall, Frances, and Williams, C.T. (Eds.), *Rare Earth Minerals—Chemistry, Origin and Ore Deposits*: London, United Kingdom, Chapman and Hall, The Mineralogical Society, Series 7, 193–225.
- Zaitsev, A.N., Wall, F., Le Bas, M.J., 1998. REE-Sr-Ba minerals from the Khibina carbonatites, Kola Peninsula, Russia: their mineralogy, paragenesis and evolution. *Mineral. Mag.* 62, 225–250.
- Zurevinski, S.E., Mitchell, R.H., 2004. Extreme compositional variation of pyrochlore-group minerals at the Oka carbonatite complex, Quebec: evidence of magma mixing? *Can. Mineral.* 42, 1159–1168.
- Zhang, X., Pazner, M., Duke, N., 2007. Lithologic and mineral information extraction for gold exploration using ASTER data in the south Chocolate Mountains (California). *Photogrammetry Remote Sens.* 62, 271–282.